# Studies of Interface Deformations in Single- and Multi-Layered Liquid Baths Due to an Impinging Gas Jet

F. QIAN, R. MUTHARASAN, and B. FAROUK

An impinging gas jet on a molten bath having a slag layer on top is encountered in various metal processing operations. The impinging region was studied using a physical model consisting of an air jet and water bath. Kerosene and corn oil were used as the second layer to investigate the role of the slag layer properties on interface shape and bath circulation. The interface shapes were measured both photographically and by using a surface-tracking resistance probe. The limiting condition at which the jet breaks through the kerosene or corn oil layer and reaches the water layer was determined experimentally. A phenomenological model for the prediction of penetration depth is developed for both short and long jet heights for liquid baths with and without a second liquid layer on top.

## I. INTRODUCTION

AN impinging gas jet on molten metal baths is commonly encountered in such processes as basic oxygen furnace (BOF) and electric arc furnaces (EAF). A protective slag layer is usually found over the molten metal bath in such cases. Knowledge of interface shapes and local fluid flow fields in the impinging region is important for characterizing the interaction of the metal bath with the surroundings. Most published articles to date have focused on the impinging gas jet on a single liquid bath, while in practice, two liquid layers are encountered. For example, Matthieu,[1] Maatsch,[2] and Banks and Chandrasekhara[3] performed experiments with impinging air jet on a single liquid bath of water, and Cheslak *et al.*[4] conducted measurements of liquid surface deformation using two separate experimental models, *viz.* an axisymmetric impinging air jet on water and again on fast setting cement. The latter approach preserved the interface shape so that approximate measurement of the interface shape could be made. Wakelin[5] examined the interactions between gas jets and the surfaces of liquids, including molten metals. The experimental investigation again involved an air jet impinging on a single liquid bath. The focus of the study was on the effect of the jet characteristics on the size and shape of the depression formed in the liquid, bath circulation, mass transfer rate, and conditions at which splashing occurs. In addition, characterization of the flow field induced by the jet in the liquid bath was also made. Photographic studies showed that the liquid at the interface moved rapidly toward the vessel wall, and the return flow caused the formation of a toroidal vortex. Although Wakelin's study yielded important insights into the impinging jet problem, his study was limited to a single-layer liquid bath.

In the BOF or EAF process, a gas jet (oxygen) entrains and reacts with the surrounding gas and molten liquids (slag or metal) and exchanges mass momentum and heat with them. The temperature, density, and compositions of the jet also vary along its path. Sharma *et al.*[6] studied the jet penetration and bath circulation in a 200-lb BOF. They found that the depth of jet penetration was solely governed by the mechanical forces of the oxygen jet. The bath circulation was also mainly driven by the oxygen jet force. Careful study of the literature indicates that influence of the top slag layer properties on the local transport phenomena has not been investigated for these types of processing situations. The present study is considered to be a first step in systematically investigating the effects of the upper layer liquid properties on the interface shape and flow behavior in a two-layer liquid bath driven by an impinging gas jet.

Only a few studies consider an impinging jet on a two-liquid layer bath. Turkdogan[7] examined photographically the phenomenon of ''emulsion'' formation. His goal was to better understand the mechanism of formation of metal droplets dispersed in slags of open-hearth steelmaking processes and more importantly in BOF. In these processes, metal droplets are formed and dispersed in the slag layer due to the impinging gas jets, as well as rising gas bubbles. It was believed that rising bubbles will carry with them a small amount of metal into the slag layer, where they become entrained by surface tension forces. It was found that at low impinging jet velocities, no emulsification occurred, while at high jet momentum, oil and water layers became emulsified at the interface. The condition at which this occurred was when the top liquid layer was completely penetrated by the jet to reach the liquid bath beneath it. He and Standish[8,9] studied liquid droplet generation due to gas jet impingement using water and glycerin/mercury models. Although Turkdogan and He and Standish[8,9] provided insights into the nature of the droplet formation due to impinging jet, measurements of deformation were not performed and the effect of transport properties of the slag layer on liquid metal circulation was not investigated.

In this article, using a physical model consisting of an air jet and water bath, with kerosene or corn oil as a second layer over the water, interface shapes and penetration depths are characterized based on fundamental process variables. Effects of the transport properties of the two liquids (kerosene and corn oil) on the interface shapes and flow fields are also experimentally determined under various im-

F. QIAN, Graduate Student, Mechanical Engineering Department, R. MUTHARASAN, Professor, Chemical Engineering Department, and B. FAROUK, Professor, Mechanical Engineering Department, are with Drexel University, Philadelphia, PA 19104.

Manuscript submitted January 9, 1995.

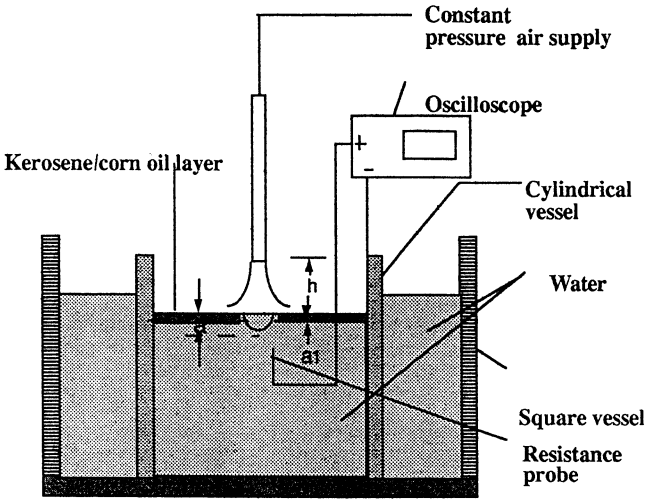


Fig. 1—Experimental arrangement.

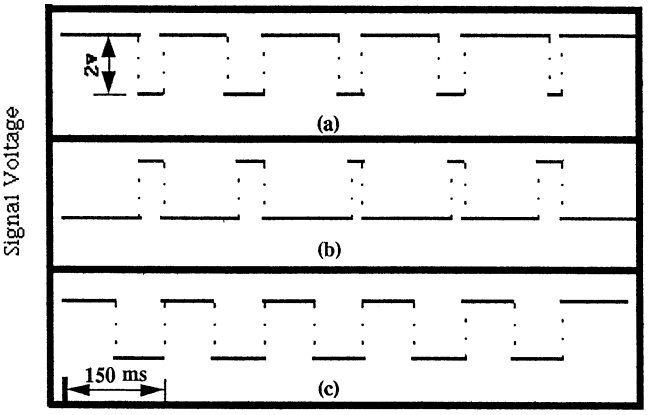


Fig. 2—(*a*) through (*c*) The probe signal recorded by an oscilloscope.

pinging jet conditions, namely, jet diameter, jet height, and jet momentum. A formulation for predicting penetration depth for both short and long jet height ranges is established based on process parameters. An existing model by Wakelin[5] was extended to incorporate both short and long jet heights.

## II. EXPERIMENTAL METHODOLOGY

### A. *Apparatus*

The experimental facility used is shown in Figure 1. It mainly consists of a cylindrical glass vessel that contains the liquids (corn oil/water or kerosene/water), a flow rate meter and flow control valves, a jet nozzle which generates the gas jet, and a traversing mechanism which carries an electroresistivity probe to measure the position of the interfaces. The aim of the experiments was to determine the interface geometries for a range of impingement conditions. The cylindrical glass vessel is 29.8 cm in diameter and 20.3 cm in depth. Optical distortion due to the circular surface was eliminated by placing the vessel in a square glass cylinder also filled with water. A U-shaped resistivity probe (Figure 1) is designed such that it does not interfere with the jet flow field. The electroresistivity probe works like a switch. The probe is insulated except at the tip region. When the tip submerges in water, the switch is ''on'' since water is conductive; when the tip is in air, the switch is ''off.'' The details about the probe were given by Turkoglu and Farouk.[10] The interface region is detected by a change in the output (voltage) of the probe signal.

When the jet momentum is greater than a certain critical value, oscillations of the interface have been observed. For an oscillating interface, the probe signal also fluctuates. In such cases, an attempt was made to measure the mean location of the interface. Figures 2(a) through (c) are representative probe signals recorded by an oscilloscope for a fluctuating air/water interface. The width of the upper line of the signal represents the time when the tip of the probe is in the water. The width of the lower line of the signal represents the time when the tip of the probe is in air. For oscillating interfaces, the signal traces as shown in Figures 2(a) and (b) indicate that the probe position is at a location either lower or higher than the mean interface location. The probe tip is at the mean interface location for the signal trace shown in Figure 2(c).

Flow visualization studies were conducted to characterize the interface shapes for the single-layer and two-layer liquid baths. The illumination light was provided from the back of the bath and a Nikon SLR camera was used to record the images on high speed photographic film.

### B. *Procedure*

First, the air/water interface due to the impinging gas jet was studied with no second layer. All experiments were conducted at room temperature (293 K). The three nozzles used were of diameters 0.58, 1.2, and 2.3 cm, respectively. The distance of the nozzle exit from the undisturbed water surface varied from 1.5 to 21 cm in the experiments. For each of the experimental cases, a range of flow rates from 0.5 to 12.5 SCMH was considered for investigating the interface shape. The range of air flow rate and nozzle diameters was selected to avoid the gas dispersion region. At high gas flow rates, gas is injected into the liquid pool, resulting in dispersion in the liquid phase. Although this region of operation is important from a practical viewpoint, under such conditions, the interface shape is very oscillatory, obviating reproducible depression measurements. Since our objective is to first establish the nature of interface shape and the nature of flow field at the interface, all experiments were limited to the momentum transfer region, wherein the interface shape showed no or little interface oscillation. Kerosene/water and corn oil/water systems subjected to impinging gas jets were studied next. A thin layer of kerosene or corn oil was laid over the water surface to simulate metal/slag layer interaction as found in metal processing and refining. The interface shapes (gas/liquid and liquid/liquid) behave quite differently from the interface shapes observed with a single liquid layer. Corn oil has a viscosity of 46 cp, while kerosene has a viscosity 1.5 cp, and the viscosity of water is 1.0 cp at 293 K. Correspondingly, corn oil density is 0.86 g/cm$^3$, kerosene density is 0.81 g/cm$^3$, and water density is 0.99 g/cm$^3$. Typical values of viscosity of slag and steel are 200 and 6 cp, respectively. The ratio of momentum diffusivity of kerosene to water is about 1.9, for corn oil to water 55, and for slag to steel melts about 900. Although the corn oil/water system has a significantly lower momentum diffusivity ratio compared to

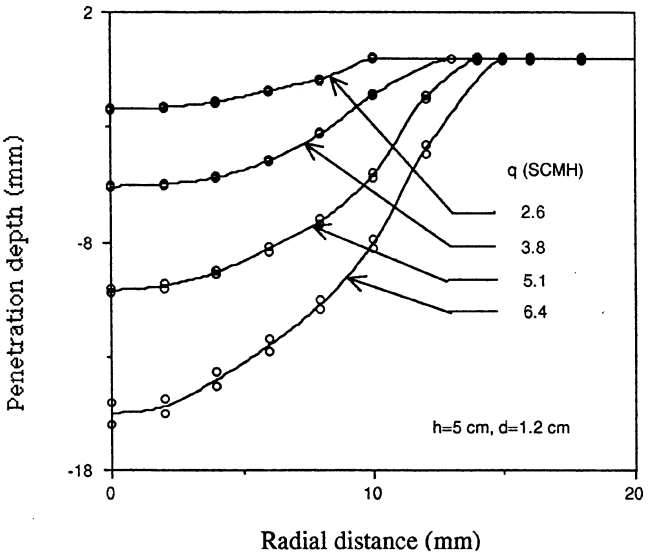


Fig. 3—Effect of air flow rate on interface shape (and deviation error) for a single-layer liquid bath at a jet height of 5 cm and jet diameter of 1.2 cm.

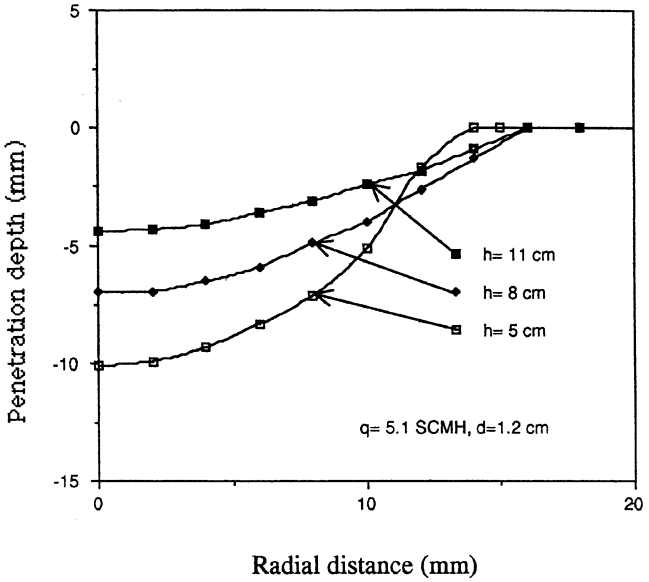


Fig. 4—Effect of jet height on interface shape for a single-layer liquid bath at a jet flow rate of 5.1 SCMH and jet diameter of 1.2 cm.

the slag/steel system, it is illustrative to examine the differences brought about in the interface behavior when the ratio is increased from a value of 1.9 (kerosene/water) to 55 (corn oil/water). The viscosity ratio of corn oil to water is 460, for kerosene to water 1.5, and for slag to steel 33. In this case, the slag/steel case is between the bounds of the two model systems. The momentum diffusivity ratio may be useful in determining the rate of change that is brought about on the flow field, while the viscosity ratio is indicative of interface shape.

For the present experiments, the thickness of the kerosene or corn oil layer was kept constant at 0.8 cm. The diameter of the nozzle used was 1.2 cm. The flow rate was varied from 1.8 to 9.2 SCMH. The height of the nozzle was set at 3.0, 5.0, and 7.0 cm.

## III. EXPERIMENTAL RESULTS

### A. *Single-Layer Liquid Bath*

An initial set of experiments was conducted with a single-layer liquid bath using three different jet diameters at a variety of jet heights. Typical results obtained are given in Figure 3 for the interface shape as a function of radial distance for different air flow rates for a 1.2-cm diameter jet located 5 cm above the initial interface position. The maximum depth of the interface (at the stagnation region) increases from 0.22 cm to nearly 1.60 cm as the gas flow rate $q$ increases from 2.6 to 6.4 SCMH. The centerline depression is seen to be nonlinearly related to the impinging air flow rate. For a twofold increase in flow rate, the centerline depression increased by nearly threefold. The width of the depression also increased nonlinearly with the air flow rate. The repeatability of the experiments was found to be satisfactory. The maximum deviation of each measurement point is also shown in Figure 3 by using two small circles bounding the average point in the curve. The maximum value of the deviation error of the measurement increased from 0.04 to 0.5 mm as the flow rate increased from 2.6 to 6.4 SCMH. Similar deviations were also observed at other jet heights and diameters (0.58 and 2.3 cm, respectively).

In Figure 4, the effect of the jet height on the interface shape is given for the 1.2-cm-diameter jet at a flow rate of 5.1 SCMH. At lower jet heights, the penetration is deeper, as expected, since the centerline velocity of the jet is higher; but the diameter of the crater formed is smallest since the diameter of the jet column is smaller. At higher jet heights, the centerline velocity of the jet at the impingement region will decrease and the diameter of the jet column will increase, so the penetration is shallower but with a larger diameter. Thus, the three curves in Figure 4 intersect one another. For a larger diameter jet at the same flow rate, the interface depression was lower as well.

Figure 5 shows the interface shape photographs for the single-layer (air/water) bath for three jet flow rates. The distance between the jet exit and the undisturbed liquid surface was maintained at 2.5 cm. Figure 5(a) shows the flat interface for the no jet flow case. The dark portion in the figures (under the jet nozzle) shows the penetration cavity formed in the water surface due to the air jet. As the jet flow rate increases from 2.7 to 3.2 SCMH, the penetration depth of the cavity increases significantly.

### B. *Two-Layer Liquid Bath*

Experiments similar to those performed for the air/water system were repeated with a second layer of liquid on top of the water. Figure 6 summarizes the major results of the interface shape for different air flow rates (in the range of 2.6 to 5.7 SCMH) for the case of kerosene used as the second layer. The distance between the jet exit and the undisturbed kerosene layer was 3.0 cm. As the impinging gas flow rate is increased, the kerosene layer goes through increasing levels of deformation until it is reduced to zero thickness at the impingement location. For an air flow rate less than 3.1 SCMH, the kerosene/water interface remained flat, indicating that the shear exerted by kerosene on the water phase was not significant. The kerosene layer penetration and the entertainment behavior are initiated at 3.1

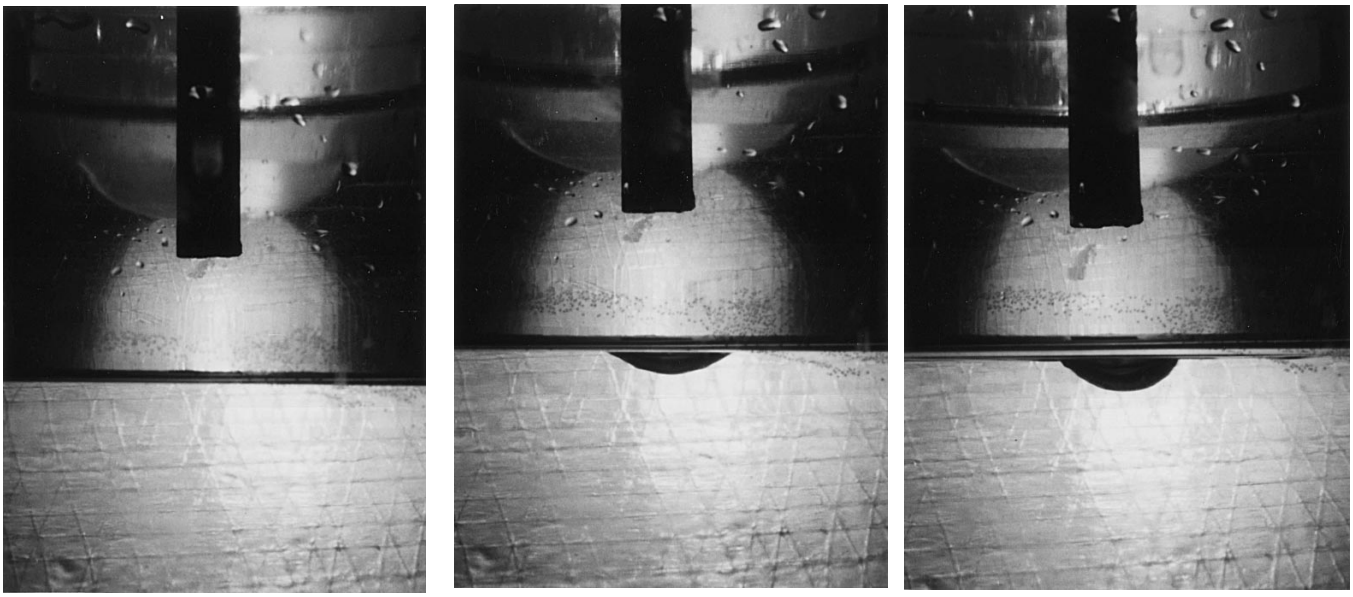

(*a*) q = 0.0 SCMH (*b*) q = 2.7 SCMH (*c*) q = 3.2 SCMH

Fig. 5—(*a*) through (*c*) Photographs of air jet penetration into water bath.

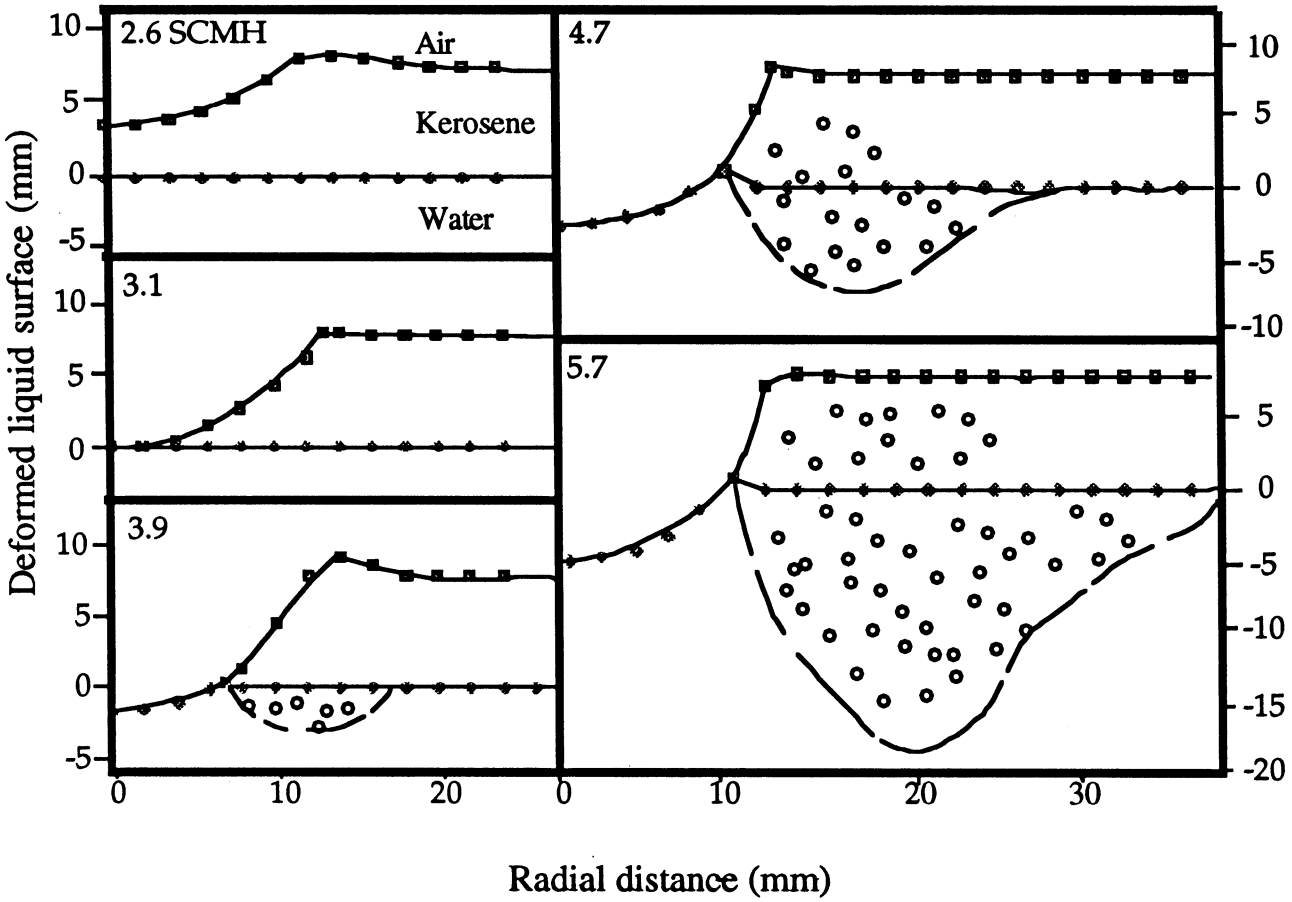


Fig. 6—Effect of increasing air jet flow rate on the gas/liquid and liquid/liquid interfaces for the multilayer (kerosene/water) bath. (The broken line represents the boundary of the emulsion region.)

SCMH. Under these conditions, the crater created by the jet was not stationary due to high levels of turbulence. The interface shapes plotted in the figures are averaged values measured over a period of 100 seconds, which was significantly longer than the timescale of oscillations. Beyond this flow rate, the air jet penetrates the water bath also causing entrainment of water droplets and air bubbles in the kerosene layer. The region within which entrainment was

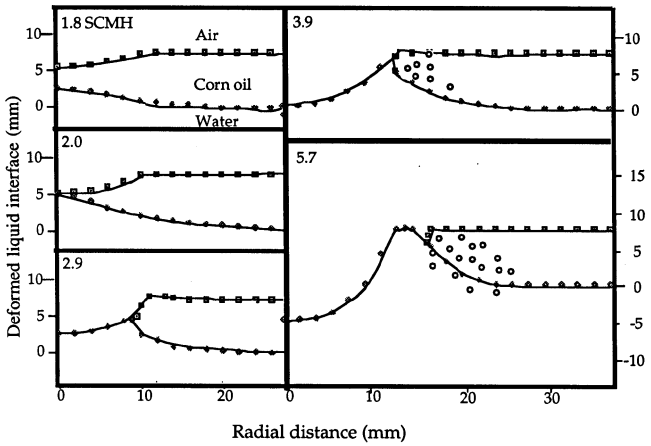


Fig. 7—Effect of increasing air jet flow rate on the gas/liquid and liquid/liquid interfaces for the two-layer (corn oil/water) bath.

observed is noted by the dashed lines in Figure 6. The air bubbles formed in the water phase exhibited two types of behavior. The large bubbles, greater than 3 mm (approximately), rose from the water phase and broke through the water/kerosene interface and exited through the kerosene/air interface. Very small air bubbles, with diameters less than 1 mm (approximately), seemed to accumulate in the water/kerosene interface, presumably, immobilized due to surface tension forces being greater than buoyant forces. At the highest flow rate, 5.7 SCMH (Figure 6), the width of the exposed water area became larger and the depth of air penetration became deeper. Under these conditions, the bubbly region increased significantly, as noted in the figure.

Similar experiments were then carried out using corn oil instead of kerosene to investigate the influence of viscosity of the second layer on the nature of interface shape. Typical results obtained are summarized in Figure 7. One significant difference due to the high viscosity of corn oil is evident by the shape of corn oil/water interface shape. Even at a low air flow rate of 1.8 SCMH, the corn oil/water interface is lifted up in the jet region, indicating that the shear imparted to the corn oil by the air jet is transmitted to the corn oil/water interface because of corn oil's high viscosity. As the air flow rate is increased to 2.0 SCMH, the oil layer thickness is reduced to near zero value at the jet axis region. This flow rate is significantly smaller than the flow rate of 3.2 SCMH, at which the kerosene layer was reduced to a near zero value at the jet axis. The depression of the corn oil layer surface was 2.84 mm, while the rise in the height of the water surface was 5.1 mm. Unlike the kerosene case, further increase in air flow rate did not cause entrainment of water droplets or air bubbles. Such entrainment was observed only when the flow rate reached a value of 3.0 SCMH, as shown in Figure 7. At this flow rate, the jet penetration depth was 4.9 mm and a few air bubbles were formed which entered the corn oil layer in the region where the three phases meet. When the air flow rate was further increased to 3.9 SCMH, the depth of penetration increased to 7.64 mm. The amount of entrained bubbles increased as well, but the quantity and size of the bubbles were less than those formed in the kerosene layer case. As shown in the figure, the surface of the water layer rose to nearly the same height as in the oil layer.

Figures 8 and 9 show the interface shape photographs (gas/liquid and liquid/liquid) in the bath due to gas jet impingement for the corn kerosene/water and oil/water baths, respectively. For both cases, the distance between the nozzle exit and the undisturbed liquid surface was kept at 2.0 cm. For the flow visualization studies, the jet flow rate was varied from 0.0 to 3.1 SCMH for the kerosene/water case and from 0.0 SCMH (no jet flow) to 2.9 SCMH for the corn oil/water case. For the kerosene/water layer case, the second layer is pushed back with increasing jet velocity, as shown in Figure 8. The kerosene/water layer remains essentially undisturbed. Figure 9(a) shows the case for no jet flow where both the air/corn oil and corn oil/water interfaces are flat. As the jet flow increases, the corn oil surfaces are deformed near the impingement area. Due to the high viscosity of the corn oil layer, the corn oil/water interface begins to deform also and the interface is pulled up due to the shear driven flow in the corn oil layer. The two interfaces eventually meet and the water layer becomes exposed to the air jet. Similar observations were also reached by the probe measurement studies, as reported in Figure 7.

## IV. CORRELATIONS FOR PENETRATION DEPTH PREDICTION

The experimental data collected (using the interface tracking resistance probe) were compared with existing correlations. Improvements to the existing correlations were suggested such that both short and long jet height data can be accommodated. Attempts were also made to correlate the two-layer liquid bath data obtained in this study.

### A. *Single-Layer Liquid Bath*

The Nomenclature used in this section follow the earlier studies by Cheslak *et al.*[4] and Wakelin.[5] Consider a gas jet of diameter $d_j$ located a distance $h$ from the undisturbed surface of the liquid bath, issuing at a velocity $V_j$ (Figure 1). If the surface tension and shear on the cavity wall are neglected, the gas penetration into the liquid is determined by the dynamic pressure associated with the centerline velocity of a free, turbulent, incompressible jet. In order to determine the dynamic pressure, we need a relationship for velocity of the jet at the gas-liquid interface. The centerline velocity $V_c$ at the surface level of the liquid can be obtained from (assuming free jet behavior)

$$\frac{V_C}{V_j} = \frac{K_2 d_j}{h + a} \qquad [1]$$

where $K_2$ is an experimentally determined constant and the variable $a$ is the penetration depth, as shown in Figure 1. The value of the constant $K_2$ has been reported to be 6.4 (Albertson *et al.*[11] and Farris[12]) and by some authors as 7.5 (Szekeley[13]) for axisymmetric jets. Application of energy balance principles to the case of a single-layer liquid bath gives (Banks and Chandrasekhara[3] and Cheslak *et al.*[4])

$$\frac{M}{\gamma_L h^3} = \frac{\pi}{2K_2^2} \left(\frac{a}{h}\right)\left(1 + \frac{a}{h}\right)^2 \qquad [2]$$

where $\gamma_L$ is the density of the liquid and $M$ is the jet momentum given by

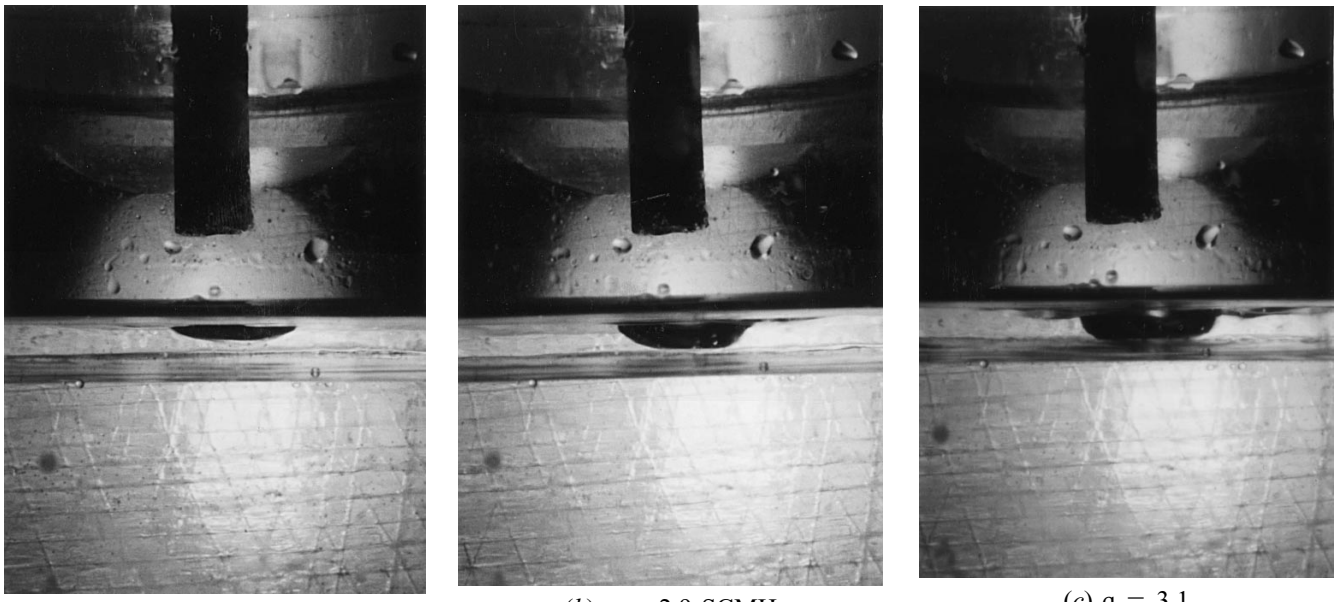

(*a*) q = 2.6 SCMH (*b*) q = 2.9 SCMH (*c*) q = 3.1

Fig. 8—(*a*) through (*c*) Photographs of air jet penetration into water bath with a kerosene layer.

$$M = \rho_g \frac{\pi}{4} d_j^2 V_j^2 \quad [3]$$

Interface depression data obtained in the single-layer liquid bath experiment are plotted as a function of dimensionless jet momentum in Figure 10. The diameter of the jet is 1.2 cm, while the jet height varied from 3 to 7 cm. In the same plot, the relationship proposed by Cheslak *et al.*[4] and Wakelin[5] is also presented. The existing models appear to overpredict the magnitude of interface depression over the range of jet momentum examined. In the original investigation, Cheslak *et al.* obtained all of their data for comparison with theory from experiments conducted with a single small diameter air jet of 1.4 mm in different liquid systems: mercury, acetylene tetrabromide, glycerin, and trichloro-ethane liquid baths. The range of *h/dj* values explored was large and over 10. Wakelin also used a small diameter nozzle (estimated as 3 mm) in $CO_2$/water, $CO_2$/mercury, air/water, and air/mercury systems. The range of *h/dj* values explored was also large and over 10. Similar results for a larger jet diameter ($d_j$ = 2.3 cm) are shown in Figure 11. The jet height varies from 3 to 9 cm in this case. It appears that the cause of deviation for low *h/dj* jets is in using the centerline velocity for determining the kinetic energy of the gas jet. As large radial velocity gradients exist in 1.2- and 2.3-cm-diameter jets (as studied here) compared to the smaller diameter jets used by earlier workers, the energy balance model of Cheslak *et al.* overpredicts the depth of penetration.

### B. *Two-Layer Liquid Bath*

The case with two liquid layers is considered next. Application of the energy balance at the bottom of the depression gives

$$\gamma_{L1} a_1 + \max\left[\gamma_{L2}(a - a_1),\ \gamma_{L1}(a - a_1)\right] = \frac{1}{2}\rho_g V_c^2 \quad [4]$$

where $\rho_g$ is the density of the gas, $\gamma_{L1}$ is the specific weight of the liquid in the top layer, $\gamma_{L2}$ is the specific weight of the liquid in the bottom layer, and $a_1$ is the thickness of the top liquid layer (Figure 1). Applying energy balance, the nondimensional momentum can now be expressed as

$$\frac{M}{\gamma_{Lmix} h^3} = \frac{\pi}{2K_2^2}\left(\frac{a}{h}\right)\left(1 + \frac{a}{h}\right)^2 \quad [5]$$

where

$$\gamma_{Lmix} = \frac{a_1}{a}\gamma_{L1} + \max\left[\gamma_{L1}\left(1 - \frac{a_1}{a}\right),\ \gamma_{L2}\left(1 - \frac{a_1}{a}\right)\right]$$

Equation [5] is an extension of the single liquid formulation for the case of two liquids following Cheslak *et al.*[4]

The penetration depths measured in the two-layer liquid system are compared as a function of jet momentum in Figures 12 and 13 for the two cases of kerosene/water and corn oil/water, respectively. In the same figures, predicted penetration is also plotted using the model given in Eq. [5]. The two lines in the figures correspond to the two $K_2$ values reported in the literature, *viz.* 6.4 and 7.5. In both instances, theory predicts the overall trend well. However, it overpredicts the magnitude of penetration, specifically for short jet heights. At different jet momentums, the penetration depth behaves very much like a single liquid bath as the jet interacts with the two-layer system. This behavior is in agreement with previous findings for a single liquid bath system, *i.e.*, the depth of penetration is independent of liquid viscosity (Cheslak *et al.*[4]).

## V. AN IMPROVED CORRELATION FOR PENETRATION DEPTH PREDICTION

According to the comparison of the experimental data with the existing models previously discussed, a modification is needed to correlate the penetration depth for a wider range of jet flow parameters. Considering a free, turbulent, incompressible jet, there are three regions that need to be

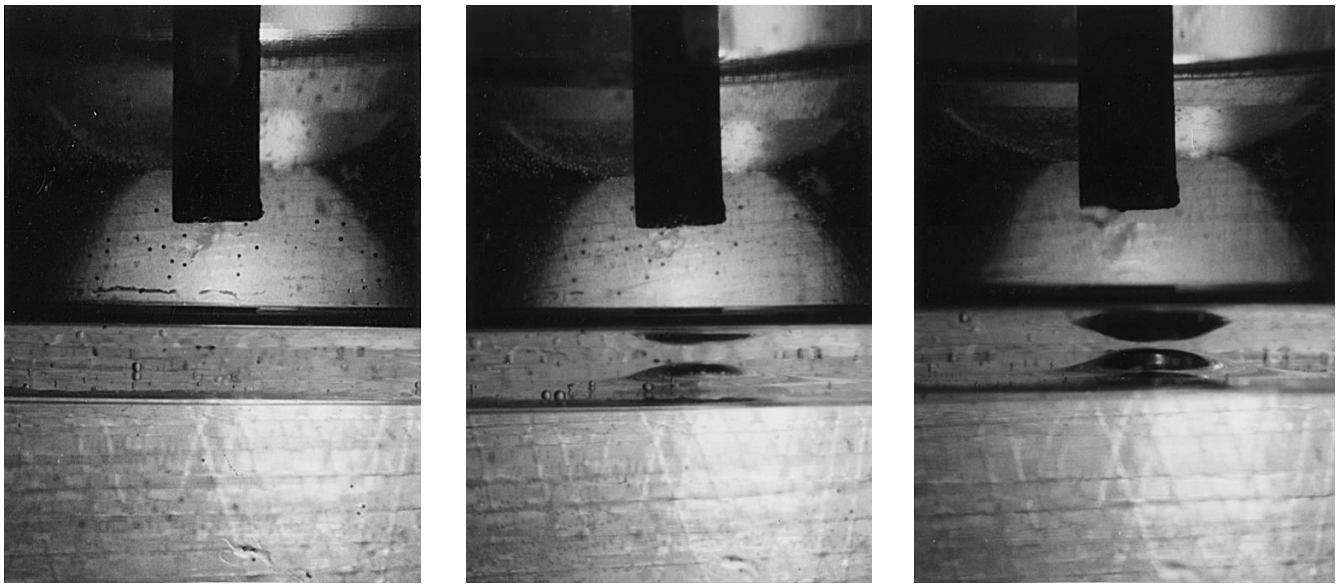

(*a*) q = 0.0 SCMH (*b*) q = 1.8 SCMH (*c*) q = 1.9 SCMH

(*d*) q = 2.0 SCMH (*e*) q = 2.9 SCMH

Fig. 9—(*a*) through (*e*) Photographs of air jet penetration into water bath with a corn oil layer.

addressed *viz.* (a) a short jet region (potential core region), (b) a transition region, and (c) a long jet region. In order to determine the dynamic pressure, we need a relationship for velocity of the jet at the gas-liquid interface. The penetration depth prediction of these three regions is discussed in Sections A through C.

### A. *Short Jet Region*

The short jet region is also defined as the potential core region, where the centerline velocity does not decay. Based on our experimental data, the following are found.

(1) The short jet region is in the range of $(h + a)/dj < 3.5$.
(2) The 1/7 power law velocity distribution[14] at the exit of the nozzle is proposed to estimate the centerline velocity $V_c$ as a function of average velocity $V_j$. Therefore, the following equation can be obtained:

$$\frac{V_C}{V_j} = 1.22 \qquad [6]$$

Based on the Bernoulli equation, the stagnation pressure of the jet at the interface is equal to the hydrostatic pressure of liquid depression. The penetration depth $a$ can be obtained from

$$\gamma_L a = \frac{1}{2} \rho_g V_c^2 \qquad [7]$$

where $M$ is the jet momentum given by

$$M = \rho \frac{\pi}{4} d_j^2 V_j^2 \qquad [8]$$

Substituting Eqs. [7] and [8] into Eq. [6], the relation be-

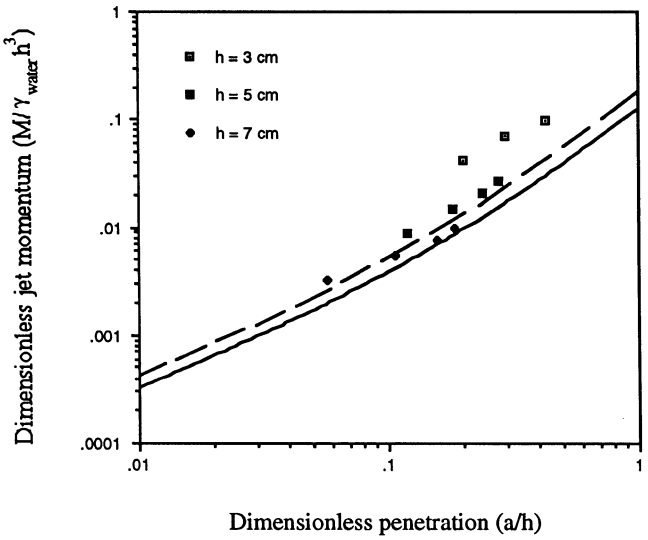


Fig. 10—Comparison of single-layer bath penetration depth ($d_j$: 1.2 cm) with model. Solid line: Cheslak *et al.*[4] ($K_2$ = 7.5); broken line: Wakelin[5] ($K_2$ = 6.4).

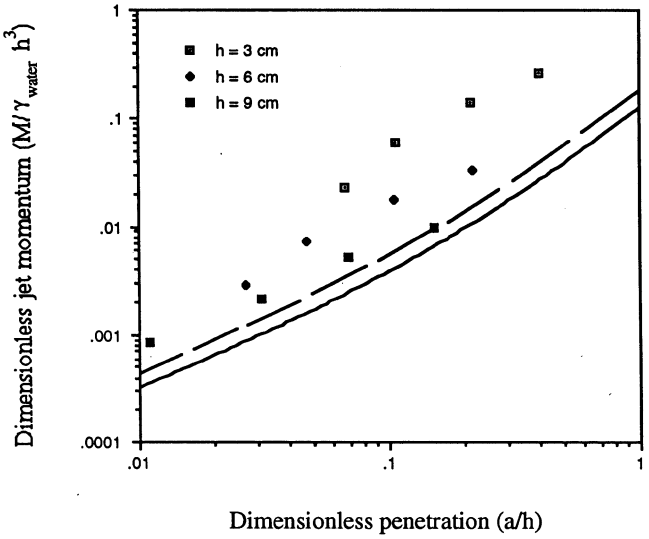


Fig. 11—Comparison of single-layer bath penetration depth ($d_j$: 2.3 cm) with model. Solid line: Cheslak *et al.*[4] ($K_2$ = 7.5); broken line: Wakelin[5] ($K_2$ = 6.4).

tween penetration $a$ and jet momentum $M$ can be expressed as

$$\frac{M}{\gamma_L a d_j^2} = 1.04 \qquad [9]$$

B. *The Transition Region*

For the transition region, the jet height is in the range of $3.5 < (h + a)/d_j < 10$. The nondimensional momentum was correlated against $(h + a)/d_j$ for best fit. The relation between penetration $a$ and jet momentum $M$ can be expressed as (for best fit of our experimental data)

$$\frac{M}{\gamma_L a d_j^2} = 0.84 + 0.0072 \frac{(h+a)}{d_j} + 0.024 \left(\frac{h+a}{d_j}\right)^2 \qquad [10]$$

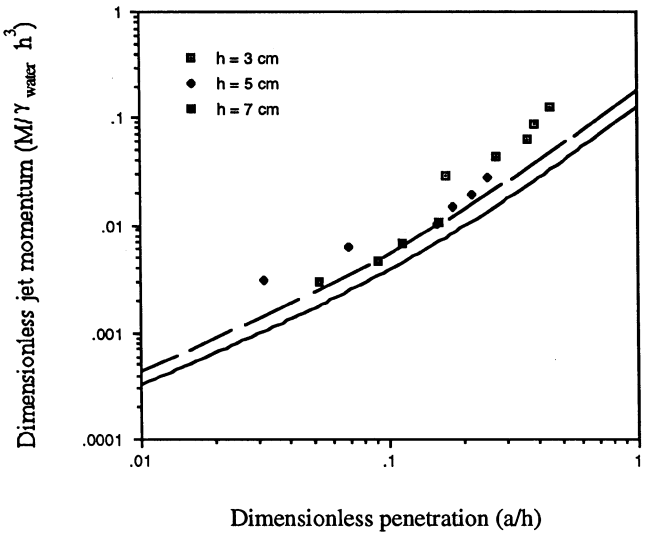


Fig. 12—Comparison of penetration depth (kerosene/water bath) with model (Eq. [5]). Solid line: $K_2$ = 7.5; broken line: $K_2$ = 6.4. $d_j$: 1.2 cm.

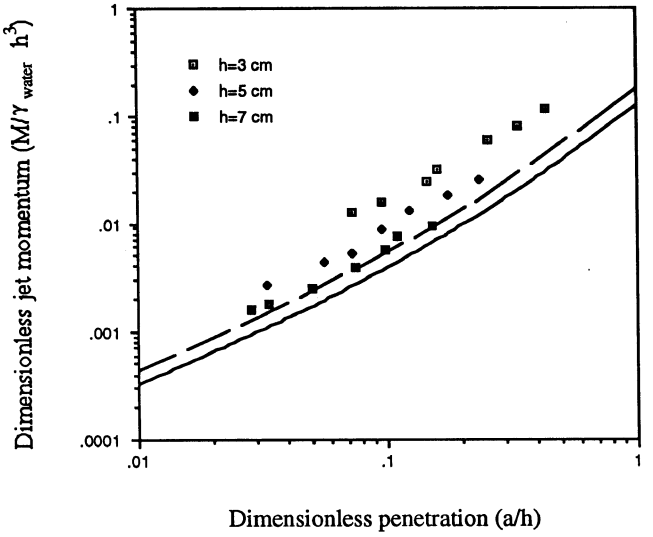


Fig. 13—Comparison of penetration depth (corn oil/water) with model (Eq. [5]). Solid line: $K_2$ = 7.5; broken line: $K_2$ = 6.4. $d_j$: 1.2 cm

C. *The Long Jet Region*

For the long jet region, the jet height is considered to be in the range of $(h + a)/d_j > 10$. The centerline velocity $V_c$ at the surface level of the liquid is given by Eq. [1] (following Cheslak *et al.*[4]). The depth of the depression can be equated to the momentum of the jet by energy balance at the bottom of the depression in the liquid layer. Application to the case of a single liquid bath gives Eq. [2], as reported earlier.

In the general form, the penetration depth prediction equation can then be written as

$$\frac{M}{\gamma_L a d_j^2} = F \qquad [11]$$

where the function $F$ may be expressed as

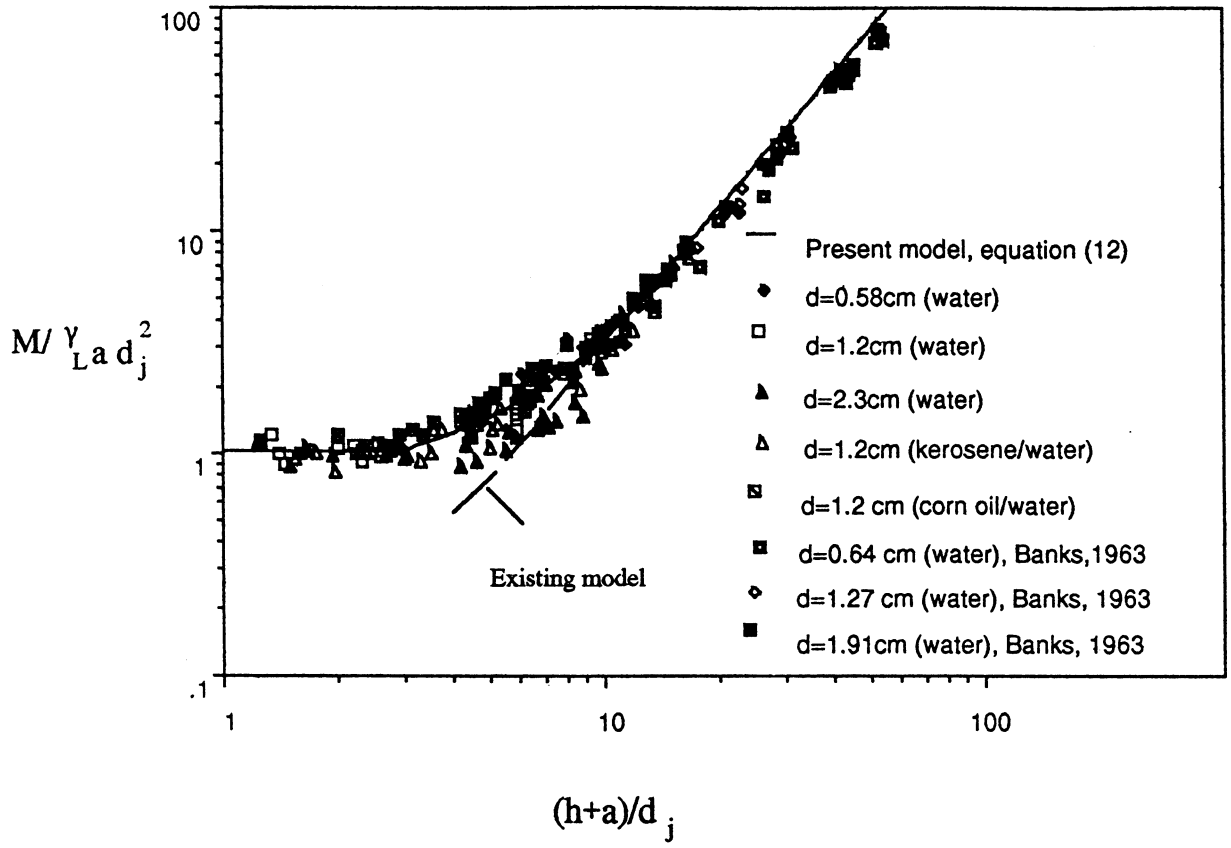


Fig. 14—Comparison of penetration depth data with proposed correlation (Eq. [12]).

$$F = 1.04 \qquad 0 < \frac{h+a}{d_j} < 3.5$$

$$F = 0.84 + 0.0072\,\frac{(h+a)}{d_j} + 0.024\,(\frac{h+a}{d_j})^2 \qquad 3.5 < \frac{h+a}{d_j} < 10$$

$$F = \frac{\pi}{2K_2^2}\,(\frac{h+a}{d_j})^2 \qquad 10 < \frac{h+a}{d_j}$$

and $K_2$ is chosen as 7.5.

Considering the case of two-layer liquid baths, a similar procedure (as used for the single-layer liquid) can be used. For the two-layer liquid systems, we propose (following Eq. [5])

$$\frac{M}{\gamma_{L\text{mix}}\, a d_j^2} = F \qquad [12]$$

where the function $F$ is as defined previously for the single-layer system. The single-layer liquid formulation (Eq. [11]) can be considered as a particular form of Eq. [12] when $\gamma_{L1}$ is equal to $\gamma_{L2}$.

All of the nondimensional penetration depth measurements $(h + a)/d_j$ (for both single-layer and two-layer systems) are plotted against the nondimensional momentum in Figure 14. The generalized correlation, Eq. [12], is also plotted in the same figure. The modified Eq. [12] compares well with the present experimental results. The experimental data under all different jet diameter, jet height, and jet momentum values studied are plotted in Figure 14. The data from Banks and Chandrasekhara[3] are also plotted for comparison. The existing model, Eq. [2], is only applicable for the range when $(h + a)/d_j < 10$.

## V. CONCLUSIONS

In this article, we have characterized the interface profiles created by an impinging jet at various values of jet momentum and jet heights for single-layer and two-layer liquid bath systems. The interface shapes were measured using a resistivity probe. The interface shape and the flowfield were also studied photographically. The influence of viscosity of the top (slag) liquid layer on the interface shape was measured and contrasted experimentally with a low (kerosene) and a high viscosity (corn oil) layer. High viscosity of the top layer causes the liquid/liquid interface to bulge up due to the jet impingement which may facilitate contact of the gas jet with the bottom layer.

A phenomenological description of the interface behavior is also given. A generalized phenomenological model was established for predicting the penetration depth for all ranges of the parameter $(h + a)/d_j$. In the short jet height region, the effect of jet velocity profile at the nozzle exit has to be considered. Based on the experimental results, it was found that the 1/7 power law[14] is a good approximation for describing the centerline jet velocity decay. For the transition region, an empirical model was formulated from the experimental data. The phenomenological model for the long jet height region was adopted from past studies. The experimental data show good agreement with the previously reported relationship.

## ACKNOWLEDGMENT

The authors wish to acknowledge partial support of this work through a grant from Lukens Steel Inc.

## REFERENCES

1. F. Matthieu: *Rev. Univ. Mines*, 1960, Ser. 9, vol. 15, pp. 1-18.
2. J. Maatsch: *Tech. Mitt. Krupp Forsch.*, 1962, vol. 20, pp. 1-12.
3. R.B. Banks and D.V. Chandrasekhara: *J. Fluid Mech.*, 1963, vol. 15, pp. 13-39.
4. F.R. Cheslak, J.A. Nicholls, and M. Sichel: *J. Fluid Mech.*, 1969, vol. 36, part 1, pp. 55-67.
5. D.H. Wakelin: Ph.D. Thesis, Imperial College, University of London, London, 1966.
6. S.K. Sharma, J.W. Hlinka, and D.W. Kern: *I&SM*, 1977, vol. 6, pp. 7-18.
7. E.T. Turkdogan: *Advances in Extractive Metallurgy*, W. Wadsworth and H.Y. Sohn, eds., Plenum Press, New York, NY, 1979.
8. Q.L. He and N. Standish: 1990, vol. 30 (5), pp. 300-06.
9. Q.L. He and N. Standish: *Iron Steel Inst. Jpn. Int.*, 1990, vol. 30 (4), pp. 305-09.
10. H. Turkoglu and B. Farouk: *ASME Winter Annual Meeting*, Dallas, TX, Nov. 1990, ASME, New York, NY, FED-vol. 100, pp. 31-38.
11. M.L. Albertson, Y.B. Dai, R.A. Jensen, and H. Rouse: *Trans. ASCE*, 1950, vol. 115, pp. 639-45.
12. G.N. Farris: Research Report No. 39, Mississippi State University, Mississippi State, MS, 1963.
13. J. Szekeley: *Fluid Flow Phenomena in Metals Processing*, Academic Press Inc., New York, NY, 1979.
14. R.M. Bruce, D.F. Young, and T.H. Okiishi: *Fluid Mechanics*, John Wiley and Sons, Inc., New York, NY, 1990.